

# Gravitational Lensing of High Redshift Type Ia Supernovae: A Probe of Medium Scale Structure

R. Benton Metcalf

*Departments of Physics and Astronomy, and Center for Particle Astrophysics  
University of California, Berkeley, California 94720*

## ABSTRACT

The dispersion in the peak luminosities of high redshift type Ia supernovae will change with redshift due to gravitational lensing. This lensing is investigated with an emphasis on the prospects of measuring it and separating it from other possible sources of redshift dependent dispersion. Measuring the lensing induced dispersion would directly constrain the power spectrum of density fluctuations on smaller length scales than are easily probed in any other way. The skew of the magnification distribution is related to the bispectrum of density fluctuations. Using cold dark matter models it is found that the amount and quality of data needed is attainable in a few years. A parameterization of the signal as a power law of the angular size distance to the supernovae is motivated by these models. This information can be used in detecting lensing, detecting other systematic changes in supernovae and calculating the uncertainties in cosmological parameter estimates.

## 1. Introduction

There is presently a large effort underway to predict and detect the weak gravitational lensing caused by Large Scale Structure (LSS) or the “cosmic shear” (see Valdes, Tyson & Jarvis 1983, Mould *et al.* 1994, Villumsen 1996, Kaiser 1992, Kaiser 1996). Such a measurement would constitute a direct probe of the mass density fluctuations on large scales irrespective of how light and baryons are distributed. This would make it possible to measure one of cosmology’s least well understood processes, how light traces mass and whether this is a function of scale. Gravitational lensing causes images to be both magnified and demagnified as well as stretched asymmetrically (shear). Most of the methods proposed for detecting LSS lensing are based on measuring the shear in high redshift galaxy images. Although the distortions in the ellipticities of individual galaxies are expected to be small they are distorted in coherent ways. Indications of lensing are sought in the alignment of the galaxy images with the assumption that they are not intrinsically aligned. This technique has already been used with great success on galaxy cluster lensing and is presently being applied to random fields in an attempt to detect the lensing effects of large scale structure. In this paper a method of detecting lensing directly through its magnification rather than shear is proposed.

The study of high redshift supernovae (SNe) is another area of cosmology and astrophysics that is seeing a lot of activity. Type Ia SNe, the brightest type of supernova (SN), are believed to be caused by the thermonuclear explosion of an accreting white dwarf. It has been found empirically that the peak magnitude of type Ia’s have a dispersion of only 0.2 - 0.3 mag in B band. It has further been found that the peak magnitude is related to the width of the SN’s light-curve which can then be used to reduce the dispersion to about 0.17 mag if one color is used (Hamuy *et al.* 1996) and 0.12 mag if multiple colors are used (Riess, Press & Kirshner 1996). In addition to the light-curve width, the SN’s color and spectral features are related to the peak luminosity (Branch, Nugent & Fisher 1997, Nugent *et al.* 1995). It may be possible to reduce this dispersion in the future by incorporating additional observables into the correction procedure.

The uniformity in type Ia SNe combined with their high luminosity makes them an excellent tool for doing cosmology. Using them to measure the redshift-luminosity distance relation has recently resulted

in tightened constraints on the cosmological parameters  $\Omega$  and  $\Omega_\Lambda$  (Perlmutter *et al.* 1997, Perlmutter *et al.* 1998, Garnavich *et al.* 1998, Riess *et al.* 1998). There are now systematic searches for Ia SNe at high redshift which can reliably discover on the order of ten SNe in a night’s observing and do spectroscopic followup (Perlmutter *et al.* 1997). In addition there are several ongoing searches for low redshift SNe. To date there have been more than 100 type Ia SNe discovered with redshifts between  $z = 0.4$  and  $0.97$  and many additional ones at lower redshift.

In this paper I concentrate on the lensing produced by dark matter composed of microscopic particles. Matter in macroscopic compact objects can cause microlensing. However, the known populations of stars will not cause a significant number of microlensing events. The microlensing of SNe has been discussed by Schneider & Wagoner (1987) and Linder, Schneider & Wagoner (1988). A SN could also be lensed by one dominant galaxy cluster or individual galaxy. There is the possibility of getting multiple observable images and high magnifications (strong lensing) in this case. It has been suggested that observing SNe behind galaxy clusters would be a way of lifting the mass sheet degeneracy that exists in shear measurements of the gravitational lensing (Kolatt & Bartelmann 1998). The likelihood of a SN at  $z = 1$  being strongly lensed by a galaxy or cluster is small unless they are specifically sought out. In general a SN will be lensed by many galaxies and larger structures, each have a weak contribution to the total magnification. This will increase the dispersion of high redshift SNe and decrease the precision of cosmological parameter determinations. This decrease in precision has been investigated by Frieman (1997) using analytic methods and by Wambsganss *et al.* (1997) using N-body simulations. Holz & Wald (1998) calculates the lensing of point sources using numerical simulations which assume that all matter is in unclustered galaxy halos. Kantowski (1998) (and Kantowski, Vaughan and Branch (1995)) does analytic calculations of this effect under the assumption that all matter is in compact objects and none of them are close enough to the line of sight to a SN to cause significant lensing. In this paper the problem will be turned around and we will ask how well the lensing itself can be determined from the SN data.

There are several important differences between the lensing of SNe and the lensing of galaxies. For SNe the signal to noise ratio in each measurement can in fact be greater. Lensing is estimated to contribute about 5 to 10% to the observed root-mean-squared ellipticity of a  $z = 1$  galaxy. For SNe the variance in the lensing contribution is comparable to the intrinsic variance in the peak magnitude at this redshift. In addition the unlensed ellipticity distribution of galaxies at high redshift is not known and can not be easily extrapolated from zero redshift galaxies. For this reason lensing must be inferred by correlations between galaxies, either between lensed galaxies or between lensed galaxies and foreground galaxies. The result is that the lensing of galaxies measures the shear averaged over a finite area on the sky. This average shear drops rapidly with increasing area and the signal to noise is reduced to something more like 1% per galaxy on the  $1 \text{ deg}^2$  scale. This is made up for by the large number of evaluable galaxies ( $\sim 10^5 \text{ deg}^{-1}$ ) to the extent that fluctuations in the projected mass density at  $1 - 100 \text{ arcmin}$  scales are expected to be detectable in the near future. In contrast, the dispersion in the absolute magnitude of type Ia SNe is presumably independent of redshift. The dispersion can then be measured in a low redshift population where lensing is not important. The lensing of galaxies does have the advantage of sources that are generally at higher redshifts where the lensing is stronger. On the other hand, the redshift distribution of faint galaxies is not strongly constrained which adds systematic uncertainty. The redshifts of SNe are individually measured.

It is clear that the lensing of SNe and the lensing of galaxies probe different scales of density fluctuations for several reasons. Because the lensing of galaxies can only be detected through correlations in their shear, or positions and shear, lensing structures that are smaller than roughly the separation between galaxies are not detectable. Since each SN is an independent measure of the lensing at a point, not an average over a region on the sky, they will be sensitive to smaller scale structures. Also the lensing of SNe is a direct measurement of the magnification which, in the weak lensing limit, is directly related to the mass density along the line of sight. The shear is dependent on the mass outside of the “beam” and thus a shear map is in a way a smoothed version of a surface density map. In the thin lens approximation the shear and the

magnification are related to each other through a differential operator (Kaiser & Squires 1993) which makes the shear insensitive to a uniform offset in the surface density - the “mass sheet degeneracy”. Although the lensing of galaxies has limitations on small scales it does have the potential of measuring lensing over a large range of scales, arcminutes to degrees. With the possible exception of SNe viewed through galaxy clusters, it will be difficult to find enough SNe that are close enough together to measure correlations in their lensing.

In the next section I describe first how the lensing of SNe is related to the density fluctuations and then I describe how the lensing signal could be identified in the data. In section 3 a specific model of structure formation is used to estimate the level of signal and to motivate some parameterizations. The last section contains conclusions and remarks about possible complications.

## 2. Formalism

In section 2.1 I show how the variance and skew of the magnification of SNe are related to the power spectrum and bispectrum of density fluctuations in the universe. In this section only a few loose and justifiable restrictions on the form of the density fluctuations will be required. In section 2.2 some formal comments are made on extracting parameters from the data and on estimating the precision with which parameters can be measured. It is assumed throughout that the lensing is weak and that multiple images are not produced. Less than one in  $\sim 10^{-3}$  SNe at  $z \sim 1$  are expected to be strongly lensed so this assumption is well justified for the redshifts considered here.

### 2.1. The Magnification

Lensing can be viewed mathematically as a mapping from points on a source plane to points on a image plane. The Jacobian matrix of this mapping can be written as the identity plus a perturbation,  $J_{ij}(\theta) = \delta_{ij} + \Phi_{ij}(\theta)$ . In the weak lensing limit the magnification is given by

$$\mu(\theta) = \det [\mathbf{I} + \Phi(\theta)]^{-1} \simeq 1 - \text{Tr}\Phi(\theta) \quad (1)$$

It is standard practice to define the convergence,  $2\kappa(\theta) \equiv -\text{Tr}\Phi(\theta)$ . The change in the magnitude of a point source is then

$$m - \bar{m} = 2.5 \log [\mu(\theta)] \simeq 2.1715\kappa(\theta). \quad (2)$$

To calculate correlations in  $\kappa(\theta)$  I will use a perturbation method based on the techniques developed in (Gunn 1967), (Blandford *et al.* 1991), Kaiser 1992. The shear tensor is given by

$$\Phi_{ij} \equiv \frac{\partial \delta \theta_i}{\partial \theta_j} = -2 \int_0^r dr' W(r, r') \phi_{,ij}(r') \quad ; \quad W(r, r_s) \equiv \frac{g(r)g(r_s - r)}{g(r_s)} \quad (3)$$

where  $r$  is the comoving radial distance and  $g(r) = \{R_c \sinh(r/R_c), r, R_c \sin(r/R_c)\}$  for the open, flat and closed global geometries respectively. The curvature scale is  $R_c = |H_o \sqrt{1 - \Omega - \Omega_\Lambda}|^{-1}$ . Subscripts with commas in front of them denote partial derivatives and  $\phi(x)$  is the potential.

The convergence will on average be zero, but it will be different for each SN. We need the correlation in the convergence of two sources at points  $\theta_1$  and  $\theta_2$  on the sky and at coordinate distances  $r_1$  and  $r_2$ .

$$\langle \kappa(\theta_1, r_1) \kappa(\theta_2, r_2) \rangle = \int_0^{r_1} dr' W(r_1, r') \int_0^{r_2} dr'' W(r_2, r'') \langle \nabla_\perp^2 \phi(\theta_1, r') \nabla_\perp^2 \phi(\theta_2, r'') \rangle \quad (4)$$

It is useful to work in Fourier space at this point. If the potential is statistically homogeneous and isotropic the power spectrum of the potential is related to its Fourier coefficients by  $P_\phi(k) = (2\pi)^3 \delta^3(\mathbf{k} - \mathbf{k}') \langle \tilde{\phi}_k \tilde{\phi}_{k'} \rangle$ .

The power spectrum of the potential is then related to the power spectrum of the mass density contrast by Poisson's equation,  $P_\phi(k, \tau) = 9a(\tau)^{-2}\Omega_o^2 H_o^4 k^{-4} P(k, \tau)/4$  where  $a(\tau)$  is the scale factor normalized to 1 at the present epoch.

The expression (4) can be significantly simplified by using an approximation that is equivalent to Limber's equation (Limber 1954), Kaiser 1992. This is a very good approximation for most realistic models of large scale structure. With this approximation equation (4) can be reduced to

$$\begin{aligned} \langle \kappa(\theta_1, r_1) \kappa(\theta_2, r_2) \rangle &= \left( \frac{3}{2} \Omega_o H_o^2 \right)^2 \int_0^{r_1 < r_2} dr' W(r_1, r') W(r_2, r') \\ &\times \int_0^\infty \frac{dk}{2\pi} a(\tau')^{-2} k P(k, \tau') J_o(g(r') |\theta_1 - \theta_2| k). \end{aligned} \quad (5)$$

where  $J_o(x)$  is the zeroth order Bessel function. The Bessel function reduces the correlations between SNe to insignificant levels unless the SNe are very close together. The variance is found by taking  $\theta_1 = \theta_2$ ,  $r_1 = r_2$ .

In a like manner the third moment of  $\kappa(r_s)$  can be expressed in terms of the bispectrum. In the case of a homogeneous and isotropic field the bispectrum can be defined by

$$\langle \tilde{\delta}(\mathbf{k}) \tilde{\delta}(\mathbf{k}') \tilde{\delta}(\mathbf{k}'') \rangle = (2\pi)^3 \delta^3(\mathbf{k} + \mathbf{k}' + \mathbf{k}'') B(k, k', \theta) \quad (6)$$

where  $\theta$  is the angle between the vectors  $\mathbf{k}$  and  $\mathbf{k}'$ . Correlations between sources will be even smaller in this case so I consider only the one point correlation. With similar assumptions to those used in getting (5), the third moment is

$$\langle \kappa(r_s)^3 \rangle = 2 \left[ \frac{3\Omega_o H_o^2}{4\pi} \right]^3 \int_0^{r_s} \left( \frac{W(r, r_s)}{a(r)} \right)^3 \int_0^\infty dk \int_0^\infty dk' \int_0^\pi d\theta k k' B(k, k', \theta, \tau). \quad (7)$$

The bispectrum on large scales (small  $k$ ) is expected to be small or zero. The third and higher moments of  $\kappa$  are dependent on significantly smaller scale structure than the second moment. Note that no assumption of Gaussianity or linear evolution of structure has been used in deriving (5) or (7).

## 2.2. Measuring Parameters

The question addressed here is how to measure the parameters of a model using the SN data. Conversely, we would also like to know the amount and quality of the data that will be necessary to measure parameters to a given accuracy. To do these things I use a likelihood analysis approach. As seen in the last section the distribution of  $\kappa$  is not expected to be Gaussian. Nonlinear clustering causes the distribution to be skewed in favor of demagnification. This is simply because the mass is concentrated into small regions so a typical line of sight will tend to travel disproportionately through underdense regions. The distribution of corrected, intrinsic magnitudes may not be Gaussian either. At present the low redshift SNe show some evidence of skewness, but are roughly consistent with Gaussian after corrections for extinction. Extinction corrections are more difficult for high redshift SNe so non-Gaussianity may be introduced in this way as well. However, with the observational errors included one might expect the distribution of  $\Delta m$  to be close to Gaussian because it is the result of several independent random processes. For the remainder of this paper I will make the simplifying assumption that  $\Delta m$  is Gaussian distributed.

The logarithm of the Gaussian likelihood function is

$$\ln \mathcal{L} = -\frac{1}{2} [\Delta \mathbf{m}^T \mathbf{C}^{-1} \Delta \mathbf{m} + \text{Tr} \ln \mathbf{C}] \quad (8)$$

$$= -\frac{1}{2} \sum_i \left[ (\Delta m_i)^2 (4.715 \langle \kappa_i^2 \rangle + (\sigma_m^2)_i)^{-1} + \ln (4.715 \langle \kappa_i^2 \rangle + (\sigma_m^2)_i) \right] \quad (9)$$

where  $\Delta m_i \equiv m_i - \bar{m}_i$ , the difference between the observed and expected magnitudes, and  $\mathbf{C}$  is the covariance matrix as predicted by the model. Expression (9) is for the special case where there are no correlations between SNe. The subscripts correspond to each of the SNe observed. I will divide the covariance matrix into two parts, the first due to lensing and the second due to other sources of dispersion in SN peak luminosities -  $C_{ij} = 4.715\langle\kappa_i\kappa_j\rangle(z) + (\sigma_m^2)_i\delta_{ij} + C_{ij}^{cor}$ . The matrix  $C_{ij}^{cor}$  has no nonzero diagonal elements and is included to account for correlations between the SN luminosities that might arise from the light-curve and/or color corrections or correlations that might arise between SNe observed on the same night or with the same telescope for example. The diagonal elements of  $C_{ij}$  are the  $\sigma_i$ 's. In turn we can divide  $(\sigma_m^2)_i = \sigma_M^2 + (\sigma_n^2)_i$  where  $\sigma_M$  is the variance in the intrinsic peak magnitude which is the same for all SNe and  $(\sigma_n^2)_i$  is the variance due to noise, light-curve fitting, etc. There is no sum over repeated indices. Maximizing (8) or (9) with respect to all the model parameters will result in the set of parameters that best fits the data. Constraints from other, independent determinations of parameters could be incorporated into the likelihood function with a prior distribution.

Now consider the problem of estimating the precision with which cosmological or model parameters will be determined. The precision can be estimated by the ensemble average of the Fisher matrix which is made of the second derivatives of the likelihood function with respect to those parameters. If we consider two parameters  $\alpha$  and  $\beta$ ,

$$\begin{aligned} \left\langle -\frac{\partial^2 \ln \mathcal{L}}{\partial \alpha \partial \beta} \right\rangle &= \langle (\alpha - \bar{\alpha})(\beta - \bar{\beta}) \rangle_{\mathcal{L}}^{-1} = \text{Tr} \left[ \bar{\mathbf{m}}_{,\alpha} \bar{\mathbf{m}}_{,\beta}^T \mathbf{C}^{-1} + \frac{1}{2} \mathbf{C}^{-1} \mathbf{C}_{,\alpha} \mathbf{C}^{-1} \mathbf{C}_{,\beta} \right] \\ &= \sum_i (4.715\langle\kappa_i^2\rangle + (\sigma_m^2)_i)^{-2} \left\{ \bar{m}_{i,\alpha} \bar{m}_{i,\beta} (4.715\langle\kappa_i^2\rangle + (\sigma_m^2)_i) + \frac{(4.715)^2}{2} \langle\kappa_i^2\rangle_{,\alpha} \langle\kappa_i^2\rangle_{,\beta} \right\} \end{aligned} \quad (10)$$

The last line is true when the SNe are statistically independent. The first terms in these expressions are the usual term that comes from uncertainties in measuring the mean magnitude of the SNe and the second term is the result of the dispersion of the magnitudes, due to lensing or other causes, being a function of the parameters being measured.

### 3. Scalings, Models and Predictions

To make some quantitative and qualitative estimates I use models whose mass density is dominated by cold dark matter (CDM). It is helpful to first consider what might be expected for the form of the lensing signal. In linear theory  $P_L(k, a(\tau)) \propto [a(\tau)g(\Omega(\tau), \Omega_\Lambda(\tau))]^2$  where  $g(\Omega, \Omega_\Lambda)$  is given in (Carroll, Press & Turner 1992). This allows the integral in (5) to decouple so that factors dependent on the power spectrum can be separated from factors dependent on cosmological parameters. The same thing happens in the opposite extreme when structure is highly nonlinear and fully virialized. In this case structure is stable in real space and the power spectrum evolves like  $P_{NL}(k, a(\tau)) \propto a(\tau)^3$  regardless of cosmological parameters. These two extreme cases can be explicitly calculated for the  $\Omega = 1$  model where  $P_L(k, a(\tau)) \propto a(\tau)^2$ ,

$$\langle\kappa(z)^2\rangle = \frac{3}{40} (r(z)H_o)^3 H_o \int_0^\infty \frac{dk}{2\pi} kP(k) \times \begin{cases} 1 & \text{linear evolution} \\ 1 - \frac{1}{2}r(z)H_o + \frac{1}{14}[r(z)H_o]^2 & \text{stable evolution} \end{cases} \quad (11)$$

where the power spectrum is evaluated at the present day. These two results bracket the real result for  $\Omega = 1$  models - linear evolution bounds it at the top and stable evolution on the bottom. The same thing can be done for  $\Omega \neq 1$  models. In this way if  $\langle\kappa^2\rangle$  is measured firm bounds on the integral of  $kP(k)$  can be found within a model. The model will already be strongly constrained by  $\bar{m}(z)$  and other observations. If the redshift dependence of  $\langle\kappa^2\rangle$  could be firmly established insight into the evolution of clustering would be gained. For  $\Omega \neq 1$  models  $P_L(k, a(\tau))$  is a somewhat steeper function of  $r(z)$  because of the decay of potential fluctuations. The stable clustering case is less strongly dependent on  $\Omega$  except for the  $\Omega^2$  factor in

(5) which comes from Poisson’s equation. The geometric factors in  $\Omega + \Omega_\Lambda \neq 1$  models will tend to make  $\langle \kappa(r)^2 \rangle$  steeper, all other things being equal.

To make things more quantitative I use the linear power spectrum of matter fluctuations given by (Sugiyama 1995):

$$P(k) = Ak^n T(ke^{\Omega_b + \Omega_b/\Omega} / \Omega h^2)^2 \quad (12)$$

$$T(q) = \frac{\ln(1+2.34q)}{2.34q} [1 + 3.89q + (16.1q)^2 + (5.46q)^3 + (6.71q)^4]^{-1/4}$$

To convert this to a nonlinear power spectrum I use the technique of Peacock & Dodds (1996) which is based on N-body simulations and thus does not take into account any hydrodynamics that could be important on small scales. In all calculations  $\Omega_b = 0.015h^{-2}$ . This power spectrum goes to  $k^{-3}$  at small scales so that the dimensionless power spectrum  $k^3 P(k)$  becomes scale independent. Figure 1 shows what range in  $k$ -space is responsible for lensing in these models. The power spectrum in this range is speculative because the Peacock & Dodds (1996) formulae which are fits to N-body simulations become less certain at small scales. I choose to cut the power spectrum off at  $k = 1000 \text{ Mpc}^{-1}$  for the purposes of (5). A cutoff at  $k = 100 \text{ Mpc}^{-1}$  reduces  $\langle \kappa^2 \rangle$  by  $\sim 10 - 18\%$ .

Motivated by (11) I find a convenient fit to the variance of the convergence in these models

$$\langle \kappa(z)^2 \rangle \simeq \eta_o^2 [r(z, \Omega, \Omega_\Lambda) H_o]^\gamma \quad (13)$$

where  $r(z, \Omega, \Omega_\Lambda)$  is the comoving distance. This fits all the  $k < 1000 \text{ Mpc}^{-1}$ , cluster-normalized CDM models reasonably well with  $\gamma \simeq 2.92$  for flat models and  $\gamma \simeq 2.80 + 0.11\Omega$  for  $\Omega_\Lambda = 0$  models as is shown in figure 2. The constant  $\eta_o$  depends on how the power spectrum is normalized. If it is normalized to cluster abundances using the formulae of (Viana & Liddle 1996) with  $h = 0.6$  I get  $\eta_o^2 \simeq (0.70 + 1.44\Omega^2)h \times 10^{-2}$  for  $\Omega_\Lambda = 0$  models and  $\eta_o^2 \simeq (0.32 + 1.80\Omega^2)h \times 10^{-2}$  for flat models. In general the convergence does not have a simple dependence on  $H_o$  because both the power spectrum’s normalization and shape are dependent on it. If the normalization is kept constant and  $\Omega$  is varied independently,  $\eta_o$  is a steeper function of  $\Omega$ , but this normalization will always be inconsistent with other observations for some range of  $\Omega$ . To properly incorporate independent constraints on the normalization (or any other parameter), a prior distribution should be incorporated in the likelihood function, (8). As is expected from the discussion above,  $\langle \kappa(z)^2 \rangle$  falls somewhere between stable and linear evolution for all the models. Here the lensing parameter  $\eta_o$  is estimated using CDM models, but this is only for the purposes of prediction. With data  $\eta_o$  can be measured. The value of  $\eta_o$  is essentially a measure of the power spectrum on small scales. The power spectrum is not very well constrained on these scales by any method that can really be called unbiased.

Figure 3 shows the angular dependence of  $\langle \kappa(\theta_1)\kappa(\theta_2) \rangle$ . The correlations between SNe will be very small if they are separated by more than about an arc-minute. It will be difficult to find enough SNe that are close enough together for this cross-correlation to be measured. The large angular sizes and high densities of galaxy clusters make them an exception to this rule, but a random line of sight is not likely to pass through a cluster. If these cross-correlations could be measured it would be sensitive to density structures of a larger scale than the diagonal elements,  $\langle \kappa_i^2 \rangle$ .

To estimate how well  $\eta_o$  can be measured we can use (10) to find

$$\langle (\eta_o - \langle \eta_o \rangle)^2 \rangle_{\mathcal{L}}^{-1} = \frac{1}{2} \sum_i \left[ \frac{9.43\eta_o(r_i H_o)^\gamma}{4.715\eta_o(r_i H_o)^\gamma + \sigma_m^2} \right]^2. \quad (14)$$

Table 1 gives estimates of the numbers of SNe needed to make a  $2\sigma$  detection of  $\langle \kappa^2 \rangle$  calculated using (10). The SNe are taken to all be at the same redshift,  $z = 0.5$ ,  $z = 1.0$  and  $z = 1.5$ . The numbers  $N_{0.10}$  and  $N_{0.13}$  are for  $\sigma_m = 0.10$  and  $0.13$ . The number goes as  $\sigma_m^4$  so it is very sensitive to this parameter. The models are intended to span the range that is consistent with cluster abundances and determinations of  $H_o$ .

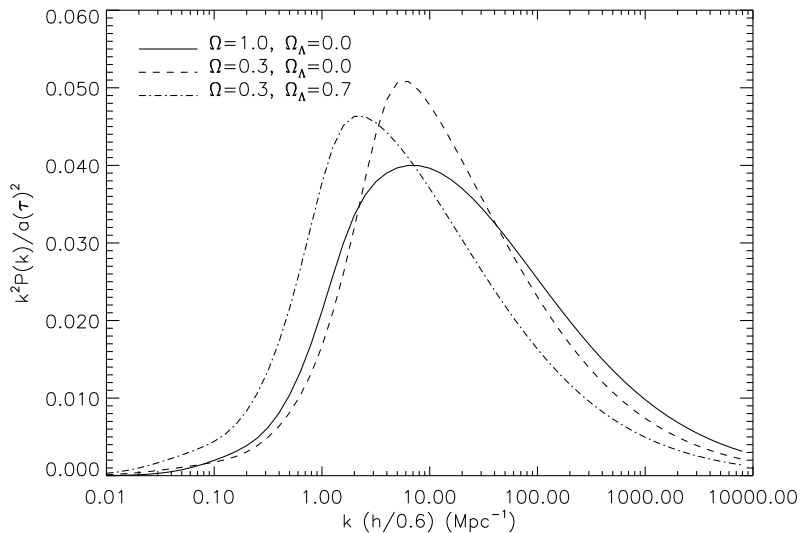


Fig. 1.— The scale dependence of the lensing of point sources in CDM models.

Table 1. Number of SNe Needed for Detection

Model				$z = 0.5$			$z = 1.0$			$z = 1.5$		
$\Omega$	$\Omega_\Lambda$	$\sigma_8$	$h$	$\Delta m$	$N_{0.10}$	$N_{0.13}$	$\Delta m$	$N_{0.10}$	$N_{0.13}$	$\Delta m$	$N_{0.10}$	$N_{0.13}$
1.0	0.0	0.6	0.60	0.04	103	261	0.08	13	27	0.11	7	11
1.0	0.0	0.6	0.75	0.05	62	153	0.09	9	17	0.13	5	8
1.0	0.0	0.5	0.65	0.03	252	668	0.06	26	59	0.09	11	22
1.0	0.0	0.8	0.65	0.06	33	76	0.11	6	10	0.16	4	5
0.3	0.0	1.0	0.60	0.03	370	995	0.06	30	69	0.08	11	23
0.3	0.0	1.0	0.75	0.03	261	694	0.06	23	50	0.09	9	17
0.3	0.0	0.7	0.65	0.02	1456	4031	0.04	97	246	0.06	31	70
0.3	0.0	1.4	0.65	0.04	89	223	0.09	10	20	0.13	5	8
0.3	0.7	1.2	0.60	0.02	592	1611	0.06	34	79	0.08	11	22
0.3	0.7	1.2	0.75	0.03	432	1165	0.06	26	59	0.09	9	18
0.3	0.7	0.8	0.65	0.02	2419	6748	0.04	114	291	0.06	31	72
0.3	0.7	1.6	0.65	0.04	139	361	0.08	11	23	0.13	5	8

Note. — These are  $2\sigma$  detection limits.  $N_{0.10}$  and  $N_{0.13}$  refer to the number of SNe needed if  $\sigma_m = 0.10$  and  $0.13$ .

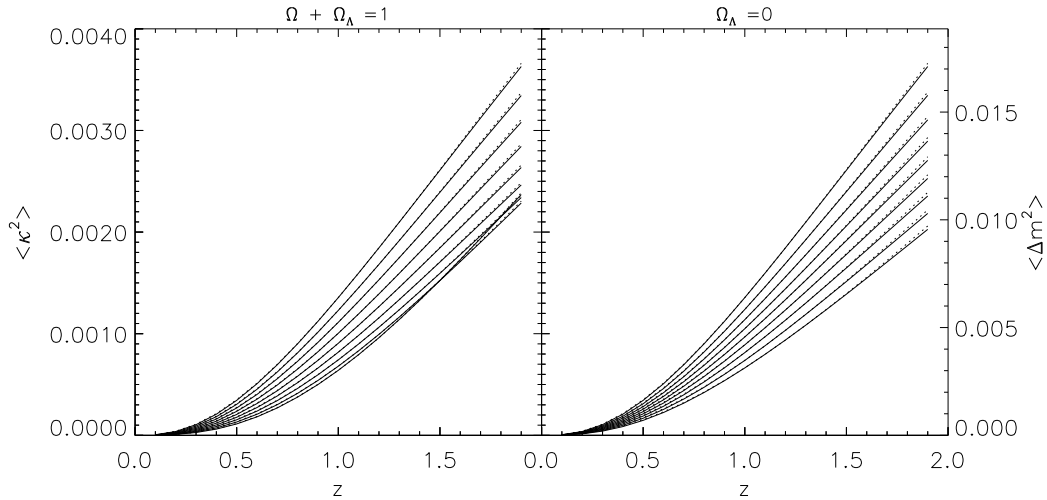


Fig. 2.— The second moment of  $\kappa$  in CDM models. On the left are flat models and on the right, open models. The dotted curves are the fits given in the text. The top curve in each plot is for  $\Omega = 1$ . Each successive curves going down has  $\Omega$  reduced by 0.1 from the one above it. All the models have the normalization that best fits galaxy cluster abundances and  $h = 0.6$ .

Of course the SNe will not all be at the same redshift and the “intrinsic” variance,  $\sigma_m$ , in the SN magnitudes will not be perfectly determined. It makes sense to try to determine both  $\sigma_m$  and  $\eta_o$  at the same time. The Fisher matrix (10) can be used to calculate an estimated error matrix. The result can be represented by an ellipsoid in parameter space. This is plotted in figure 4. The redshift distribution of the SNe is taken to be proportional to comoving volume within the redshift ranges listed. This is an idealization which assumes that the observed SN rate and the detection efficiency are not functions of redshift. A separate population of 100  $z \simeq 0$  SNe is also included. These are found by searches that target local galaxies as opposed to searches for high redshift SNe which can be done either by cataloging galaxies or by differencing multiple observations of more or less random fields. Changing the  $\sigma_8$  normalization within observational constraints has a significant effect on the number of SNe required to measure  $\eta_o$ . The  $\sigma_8$ 's listed are for the linear power spectra. Changes in the linear normalization are magnified in the nonlinear power spectrum so that they show up strongly in the lensing. Low  $\Omega$  models have significantly lower  $\eta_o$ 's than high  $\Omega$  with the same linear normalization or with cluster normalization which increases with lower  $\Omega$ . This is largely because of the factor of  $\Omega^2$  in  $\langle \kappa^2 \rangle$ . Getting to high redshift will be important for discriminating between models because the higher the redshift the less elongated the likelihood contours are along the  $\eta_o$  axis. Fifty SNe at  $1 < z < 1.5$  do substantially better at constraining  $\eta_o$  than do 100 at  $z = 0.9$ . Figure 4 also shows that simple estimates, like the ones in table 1, that do not take into account the fact that our knowledge of  $\sigma_m$  is limited can give deceptive answers. More sources are needed to detect lensing when  $\sigma_m$  is not well known because increasing  $\sigma_m$  can make a lower  $\langle \eta_o^2 \rangle$  acceptable.

The rate at which high redshift SNe can be discovered is fundamentally limited by the rate at which they occur, the area on the sky that is surveyed and the efficiency with which they can be detected. Although the rate of star formation at high redshift can be estimated from observations (Madau *et al.* 1996), the type Ia SNe are expected to lag significantly behind it. The amount of time required for a white



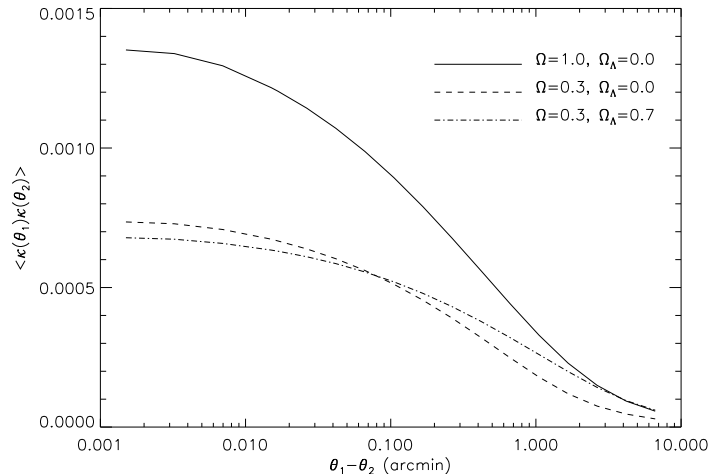


Fig. 3.— The second moment of the convergence as a function of angular separation between sources. All cases are for cluster normalized CDM models with  $h = 0.6$  and the sources are at  $z = 1$ .

dwarf to accrete enough material to go SN is not only unknown, but probably varies greatly on a case to case basis. There is one measurement of the Ia SN rate at  $z \sim 0.4$  which is  $34.4^{+23.9}_{-16.2} \text{ yr}^{-1} \text{ deg}^{-2}$  (Pain *et al.* 1996). If the rest frame rate per comoving volume remains constant the observed rate of SNe at  $z$  is  $R(z) = R_o(1+z_o)g(r(z))^2 / (1+z)g(r(z_o))^2$  which makes it 2 or 3 times larger at  $z = 1$ . More thoughtful estimations predict that the rest frame rate per comoving volume will go up by a factor of 1 to 2.5 (Sadat *et al.* 1997, Ruiz-Lapuente & Canal 1998). A SN must be detected within about a one week window in order for it to be usable. So it is reasonable to estimate that there are  $\sim 20 - 50$  usable type Ia SNe per  $\text{deg}^2$  below a redshift 1.5 at any given time. This makes detecting hundreds of high redshift SNe possible within a few years if difficulties with spectroscopic confirmation and k-corrections can be overcome.<sup>1</sup>

These calculations of  $\langle \Delta m^2 \rangle$  agree well with those of Frieman (1997). The numerical simulations of (Wambsganss *et al.* (1997), Wambsganss *et al.* (1998)) give somewhat smaller values. This is probably due to the combination of their using the COBE normalization which is smaller than the cluster normalization for low  $\Omega$  models and their simulation having a resolution of  $\sim 13h^{-1} \text{ kpc}$  ( $k \sim 480h \text{ Mpc}^{-1}$ ).

#### 4. Conclusions

It has been shown that measuring the gravitational lensing of type Ia SNe is feasible if the noise can be reasonably constrained. It would be best to solve for the best fit cosmological parameters (ie.  $\Omega$ ,  $\Omega_\Lambda$ ), lensing strength (ie.  $\eta_o$ ) and intrinsic noise ( $\sigma_M$ ) simultaneously using SNe at all redshifts. The photometric uncertainties should be comparatively well determined for each SN. One could then marginalize over the intrinsic variance,  $\sigma_M$ .

The greatest worry is of course that the type Ia SNe properties or their galactic environments are changing with redshift. Observations of spectral features and colors (Perlmutter *et al.* 1997) suggest that this is not the case, but the possibility remains. It is possible that a systematic change in the metallicity of progenitors could change both the average peak luminosity and its dispersion. Another worry is that extinction corrections change with redshift. This could systematically reduce  $\overline{m}(z)$ , increase its dispersion and make its distribution non-Gaussian. Extinction should be accompanied by reddening, which can

<sup>1</sup>The Supernova Cosmology Project (Perlmutter *et al.* 1997) currently surveys  $\sim 3 \text{ deg}^2$ .

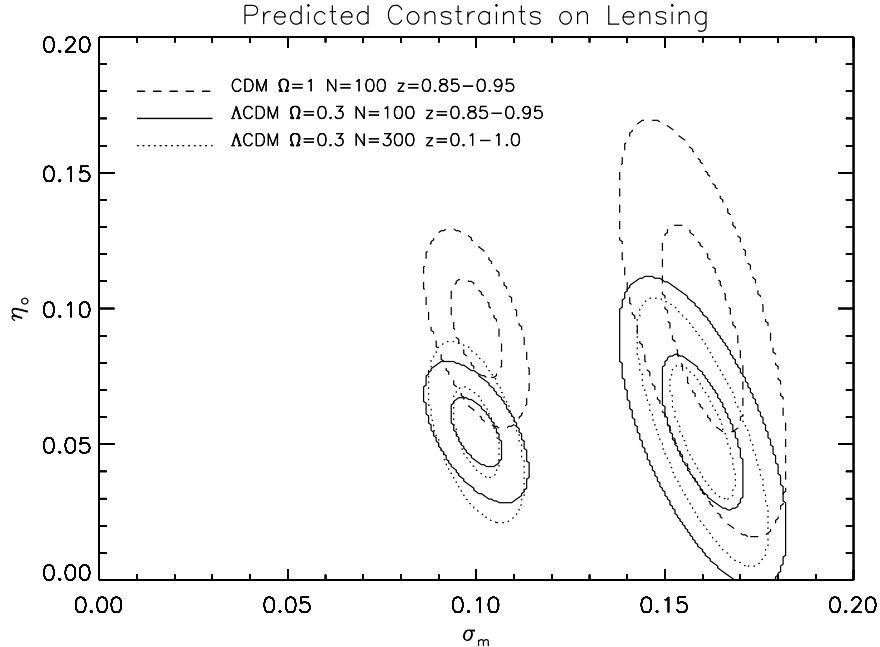


Fig. 4.— The estimated confidence regions for the combination of lensing and “intrinsic” variance in the SNe magnitudes. The number of high redshift SNe,  $N$ , are listed in the upper left along with the redshift range where they are observed. They are assumed to be distributed in redshift according to comoving volume within this range. In addition to the high redshift SNe there are assumed to be 100 “low” redshift SNe in each case which are not lensed. The inner ellipses are the estimated 68% confidence regions and the outer the 95%. The two cases for each model are with assumed  $\sigma_m = 0.1$  and  $0.16$  on the left and right respectively.

be detected, but the extinction law is not certain. These changes would affect cosmological parameter estimates as well as lensing estimates. The methods discussed here can be directly applied to detecting any redshift dependent change in the dispersion. In testing for possible redshift evolution lensing must be incorporated.

There are difficulties in searching for SNe at higher redshifts. The region of the spectrum that is used to do the light curve correction passes out of the visible at  $z \gtrsim 1$ . To go to significantly higher redshift may require switching to the IR. There is also difficulties with the K-correction and the subtraction of atmospheric lines. But with this in mind it seems that gravitational lensing of SNe could be detectable in the next few years when hundreds of high redshift SNe are observed and systematic effects are better understood. CCD cameras with fields of view approaching a square degree and very small pixel sizes are being built now. They will be used for weak lensing measurements using galaxy shear. SNe searches could be incorporated into these surveys with the benefits of improved cosmological parameter estimation and complimentary weak lensing measurements.

Combined with the limits on the cosmological parameters the lensing of SNe can constrain the power spectrum of the true mass density, unbiased by the light distribution, on the scale of galaxy halos. At present the mass distribution on these scales is not well known with the exception of within galaxy clusters which are certainly atypical regions. In this paper it has been assumed that the the large majority of matter in the universe is in the form of WIMPS or some other small particle. If the dark matter is in compact objects like MACHOs the distribution of magnifications will be different. In this way the lensing of SNe also provides information on the composition of dark matter. In addition to the variance of the magnification distribution the skewness would provide an important constraint on the nature of structure in the nonlinear

regime. A future paper will treat this subject in more detail and relate the magnification distribution to the nature of dark matter and the structure of galaxy halos.

I would like to thank J. Silk, A. Jaffe, S. Perlmutter and R. Pain for very useful discussions. This work was financially supported by NASA.

## REFERENCES

- Blandford, R.D., *et al.*, 1991, MNRAS, 251, 600.
- Branch D., Nugent P. & Fisher A., 1997, *Thermonuclear Supernovae*, ed. P. Ruiz-Lapuente, R. Canal & J. Isern (Dordrecht:Kluwer), 715.
- Carroll S.M., Press W.H. & Turner E.L., 1992, ARA&A, 30, 499.
- Frieman J.A., 1997, Comments on Astrophysics, 18, 323.
- Gunn, J.E., 1967, ApJ, 150, 737.
- Garnavich, P.M. *et al.*, 1998, ApJ, 493, L53.
- Hamuy M., Phillips M.M., Suntzeff N.B., Schommer R., Maza J. & Aviles R., 1996, ApJ, 112, 2391.
- Holz D.E. & Wald, R.M., astro-ph/9708036.
- Kaiser, N., 1992, ApJ, 388, 272.
- Kaiser, N., 1998, ApJ, 498, 26.
- Kaiser, N. & Squires G., 1993, ApJ, 404, 441.
- Kantowski R., 1998, astro-ph/9802208.
- Kantowski R., Vaughan T. & Branch D., 1995, ApJ, 447, 35.
- Kolatt T.S. & Bartelmann M., 1998, MNRAS, 296, 763.
- Limber, D.N., 1954, ApJ, 119, 665.
- Linder E.V., Schneider P. & Wagoner R.V., 1988, ApJ, 324, 786.
- Madau P. *et al.* 1996, MNRAS, 283, 1388.
- Metcalf, R B & Silk, J, 1997, ApJ, 489, 1.
- Mould, J. *et al.*, 1994, MNRAS, 271, 31.
- Nugent P., Phillips M., Baron E., Branch E. & Hauschildt P., 1995, ApJ, 455, L147.
- Pain R. *et al.*, 1996, ApJ, 473, 356.
- Peacock J.A. & Dodds S.J., 1996, MNRAS, 280, L19.
- Perlmutter S., *et al.*, 1997, ApJ, 483, 565.
- Perlmutter S., *et al.*, 1998, Nature, 391, 51.
- Pozzetti L., Bruzual A.G. & Zamorani G., 1996, MNRAS, 281, 953.

- Ruiz-Lapuente P. & Canal R., 1998, ApJ, 497, L57.
- Riess A.G., Press W.H. & Kirshner R.P., 1996, ApJ, 473, 88.
- Riess A.G. *et al.*, 1998, ApJ, 116, 1009.
- Sadat R., Blanchard A., Guiderdoni B. & Silk J., 1998, A&A, 331, L69.
- Schneider P. & Wagoner R.V., 1987, ApJ, 314, 154.
- Sugiyama N., 1995, ApJS, 100, 281.
- Valdes F., Tyson J. & Jarvis J., 1983, ApJ, 271, 431.
- Viana, P.T.P. & Liddle, A.R., 1996, MNRAS, 281, 323.
- Villumsen J.V., 1996, MNRAS, 281, 369.
- Wambsganss J., Cen R., Xu G., & Ostriker J.P., 1997, ApJ, 475, L81.
- Wambsganss J., Cen R., & Ostriker J.P., 1998, ApJ, 494, 29.